Polytechnic Journal

Polytechnic Journal

Manuscript 1744

Effects of Different Projectile Nose Shapes on the Impact Performance of the Aluminium 2024 Thin Plate

Dlair O. Ramadan

Effects of Different Projectile Nose Shapes on the Impact Performance of the Aluminium 2024 Thin Plate

Abstract

. In this study, the impact performance of the Al2024 thin plate target was determined through a numerical approach. Two different-nosed hard steel projectiles, including a blunt and a sphere, were used in order to obtain the ballistic impact of the target. ANSYS Autodyn was used to model a three-dimensional (3D) model that corresponds to a previous experimental study. The ballistic resistance of the target was numerically evaluated in terms of ballistic limit velocity, residual velocity, and energy absorption and compared at different incident angles such as 0°, 15°, and 30°. To validate the numerical outcomes, the Recht-Ipson model was used as a reference benchmark. The results of this investigation showed that when the incidence angle of a sphere-nosed projectile increased, the target's ballistic performance decreased. In contrast, the target’s ballistic resistance against a blunt-nosed projectile was little affected by the impact angle. According to the findings, the simulation results are consistent with the published numerical and experimental outcomes.

Keywords

Blunt projectile; Energy absorption; Oblique impact; Recht-Ipson model; Sphere projectile

ORIGINAL ARTICLE

Effects of Different Projectile Nose Shapes on the Impact Performance of the Aluminium 2024 Thin Plate

Dlair O. Ramadan

Department of Technical Mechanical and Energy Engineering, Erbil Technical Engineering College, Erbil Polytechnic University, Erbil, Kurdistan Region, Iraq

Abstract

In this study, the impact performance of the Al2024 thin plate target was determined through a numerical approach. Two different-nosed hard steel projectiles, including a blunt and a sphere, were used in order to obtain the ballistic impact of the target. ANSYS Autodyn was used to model a three-dimensional (3D) model that corresponds to a previous experimental study. The ballistic resistance of the target was numerically evaluated in terms of ballistic limit velocity, residual velocity, and energy absorption and compared at different incident angles such as 0°, 15°, and 30°. To validate the numerical outcomes, the Recht-Ipson model was used as a reference benchmark. The results of this investigation showed that when the incidence angle of a sphere-nosed projectile increased, the target's ballistic performance decreased. In contrast, the target's ballistic resistance against a blunt-nosed projectile was little affected by the impact angle. According to the findings, the simulation results are consistent with the published numerical and experimental outcomes.

Keywords: Blunt projectile, Energy absorption, Oblique impact, Recht-Ipson model, Sphere projectile

1. Introduction

Aluminium is widely regarded as the primary material in aircraft construction, although recent advancements have led to the utilisation of new alloys. Due to its ability to withstand the tensile forces that occur during operation, Al2024, as an alloy of aluminium, is used in the manufacturing of wing and fuselage structures [1]. In contemporary times, the significance of developing aircraft skin that can effectively withstand the impact of fragments or projectiles has become increasingly paramount.

The behaviour of metals when subjected to high-velocity impact loading can be accurately characterised by sophisticated computer codes developed for commercial purposes. These codes are equipped with sophisticated material models that enable a comprehensive understanding of the intricate behaviour involved in such scenarios. In ballistic impact issues, however, the material parameters required to simulate the consequences of elevated temperatures and high strain rates are frequently unavailable in the open literature [2,3]. In addition, there is a lack of in-depth research into numerical modelling and the evaluation of the impact of model parameters. Experimental methods are the backbone of the ballistics research community [4–6]. To identify the Al2024 target's ballistic limit with a thickness varying from 0.5 to 6.5 mm, Alfaro-Bou and Thomson [4] carried extensive ballistic experiments. The initial impact velocities of the plastic disc projectile range from 1 to 8 km/s, and its diameters are 6.4 and 9.5 mm, with masses of 10 and 30 mg, respectively. The different diameters and masses are due to the varying gun barrel inside diameter and diaphragm thickness. Levy and Goldsmith [7] as well as Goldsmith and Finnegan [5] conducted a set of experimental trials to examine the Al2024's ballistic resistance against oblique and normal

Received 29 September 2023; revised 7 November 2023; accepted 21 November 2023.
Available online 02 January 2024
E-mail address: dlair.o.ramadan@epu.edu.iq.

https://doi.org/10.59341/2707-7799.1744

impacts with hard steel projectiles at initial velocities of up to 1 km/s. Ballistic tests were performed by Gogolowski and Morgan [6] utilising targets made of 2024 aluminium that had different thicknesses (1.27, 2.54, and 3.81 mm). These targets were treated to projectiles that were circular cylinders with various fineness ratios, length to diameter ratios (0.2 and 1), and fragment simulant projectiles. The observation was made that when the thickness of the plate target increased from 2.54 to 3.81 mm, there was a transition in the failure mode of the aluminium target plate from petaling to plugging.

Kelley and Johnson [8] investigated the ballistic response of various materials against a steel projectile with a sphere-nosed shape of 12.52 mm in diameter. The materials tested included 2024 aluminium with thicknesses of 1.6, 3.18 and 6.35 mm, as well as titanium, composite, and polycarbonate targets with a thickness of 6.35 mm. The ballistic limit and failure modes were investigated for each group of targets. The study concluded that 2024 aluminium exhibited excellent results. However, further data is required for composites, polycarbonate, and titanium.

Gupta et al. [9] did both experimental tests and computer simulations (ABAQUS) to find out how different nose shapes, such as ogive, hemispherical, and blunt, as well as impact velocities and target thicknesses, affected 1100-H12 aluminium alloy plates. Ogive-nosed projectiles have been found to be the most effective when used as thin-plate penetrators because of their high level of effectiveness. It was shown that blunt-nosed projectiles required the least energy to penetrate the target plates in the case of thicker plates. In comparison to the other two projectiles, the hemispherical-nosed projectiles had the greatest ballistic limit velocity.

The research carried out by Buyuk et al. [10] involved the execution of ballistic experiments utilizing spherical projectiles on 2024 aluminium targets with different thicknesses, namely 1.58, 3.17, and 6.35 mm. The experimental ballistic limit was found for targets with thicknesses of 1.58 mm, 3.17 mm, and 6.35 mm, resulting in corresponding values of 122, 213, and 411 m/s, respectively. The aforementioned findings were effectively replicated through the utilization of finite-element simulations, showing a notable level of approval between both simulated and experimental outcomes. The performance of numerical simulations is discussed, with a particular emphasis on material characterization, mesh sensitivities, and material model parameters. It has been noticed that refinement of the mesh simply does not always result in better results in simulations with ballistic limits. This is because the interrelated factors involved in the simulation need to be carefully considered and calibrated. It was also pointed out that due to the failure mode transition changing failure and deformation using only one set of parameters is difficult. The authors Hub et al. [11] conducted experiments and a 2D numerical study to find out what the ballistic limit of Al2024_T3 with a thickness of 1.2 mm is against a projectile of 9 mm caliber pistol. In terms of residual velocities, there was a significant correlation between the numerical simulations and the experimental findings. In two separate experiments, Jones and Paik [12,13] conducted estimations on the perforation energy of aluminium plates. These estimations were based on the plates' exposure to low and intermediate impact velocities. The researchers utilized a range of empirical equations for their analysis. The findings of the study demonstrate that empirical equations have considerable importance when it comes to initial design objectives, and for the final design process, they could be sufficient in some cases.

A series of experiments were implemented by Zhan et al. [14] to investigate the impact properties of stiffened target plates when impacted by a projectile with an ogival-nosed shape. The projectiles employed in the experiment studies had beginning velocities that varied from 546 to 618 m/s. Nine different sites were used to assess the ballistic resistance of stiffened targets, and the results show strong agreement with the suggested mathematical model. Senthil et al. [15] conducted numerical simulations using the ABAQUS software to examine the ballistic impact behaviour of aluminium plates with 1 mm in thickness when exposed to ogive-tipped steel projectiles. The projectile was 15 mm in diameter and 55 g in mass. It was determined that there is a strong correlation between high-impact velocities and the existing experimental data, whereas the results were found to be underestimated at low-impact velocities.

Gara et al. [16] investigated the influence of varying impact angles ranging from 50 to 900 m/s on the impact performance of Al2024 against steel projectile. They found that the Al 2024 target exhibits the most effective energy absorption behaviour when subjected to ballistic limit velocities.

Few studies have looked examined how different constitutive models and model parameters affect ballistic reactions. Aircraft structural components including the wings, shear webs and fuselage are frequently made out of the 2024-T3 aluminium alloy. This particular alloy is chosen for its ability to provide the necessary stiffness and strength that are crucial in these applications. Aerospace structures experience various types of loads throughout their

service life, ranging from static to shock, impact, and vibration. Therefore, it is important to investigate how their structural materials respond to impact from various incident angles. There is limited availability of numerical investigations on the impact performance of the 2024 aluminium alloy at varying incident angles in the literature. The current study involved conducting numerical investigations on a 2024 aluminium plate subjected to two different noses, including a sphere and a blunt-nosed hard steel projectile with a diameter of 12.7 mm at different incident angles such as 0°, 15°, and 30°. The simulation was conducted using the ANSYS Autodyn and the Johnson–Cook elasto-viscoplastic material model, which is widely available in the literature. The numerical results obtained were then compared to the outcomes of the experiments reported in [5,7].

2. Numerical modelling

ANSYS Autodyn was used to create three-dimensional models of the target and two different-nosed projectiles, including spheres and blunts. As previously stated, the plate target was modelled using Al2024, while the projectile nose was modelled using steel. The materials utilised for both the target and projectile were obtained from the Autodyn material library and the material parameters were modified to those used by [18]. Because of the homogeneity of the target and projectiles, and to reduce processing time, the projectiles and target were modelled as quarter models with symmetric boundary conditions, as shown in Figure 1. Figure 2 shows the isometric and the side views of both the target and projectiles. The finite element simulation of the object being targeted and the two different projectiles were designed based on the geometries implemented in Levy and Goldsmith's study [7]. It's worth mentioning that Levy and Goldsmith employed three different projectiles, including sphere, blunt, and hemispherical, however the hemispherical was not included in the current study because it was outside of our focus.

Owing to their superior rigidity as compared to the thin-plate aluminium target, the projectiles were considered to have a rigid body in this study. Levy and Goldsmith verified that no lasting deformation of the projectile was detected in any of their studies. In this work, the deformable body was modelled as a circular target with certain dimensions, measuring 119.4 mm in diameter and 1.27 mm in thickness. The blunt-nose projectile had a total length and a shank diameter of 40.35 and 12.7 mm, respectively. The sphere had the same diameter (12.7 mm) [7].

The thin plate targets were divided into three distinct parts: a contact region (impact zone) and two non-contact regions, in order to speed up the computational time required for the analysis. In the contact region between the projectiles and the targets, the targets were meshed with incredibly small elements. In contrast, in the two areas where no contact was made, the aspect ratio grew larger as one moved farther from the impact point (See Figure 3). Fixed boundary constraints were applied at the periphery of the target.

3. Results and discussion

In this work, the ballistic performance of a thin, circular aluminium 2024 plate target is numerically evaluated under normal and oblique impacts with projectiles made of blunt and sphere-nosed hard steel. At 0°, 15°, and 30° impact angles, the target's ballistic resistance was investigated in terms of its ballistic limit velocity, the projectile's kinetic energy, absorbed energy by the targets, and residual velocity. The following subsections present the findings of this study.

3.1. Model validation

The current numerical model, which was built using ANSYS Autodyn, was validated by comparing the plate target's ballistic limit against the normal impact of a projectile with a blunt and spherical-nosed shape to that obtained numerically using ABAQUS/Explicit by [18], which had already been validated with experimental results obtained by [7]. The validation results are shown in Figure 4 and Figure 5. The maximum error percentage between the two models for the sphere and blunt-nosed projectile results was calculated and found to be 6 % and 13 %, respectively. This confirms the good agreement between the present and numerical results of [18].

3.2. Effects of varying obliquities

The effect of varying impact angles on the Al2024 thin plate target against the impact of a sphere and a blunt projectile was studied through numerical investigation after the simulation's precision at a normal impact angle was confirmed with Senthil et al. [18]. It was assumed that the projectiles' mass, target span, and impact velocity would be the same as those used by Levy and Goldsmith [7]. The impact angle, or obliquity, was varied at 0°, 15°, and 30°, while the thickness of the target remained fixed at 1.27 mm. The results of the varying obliquities for

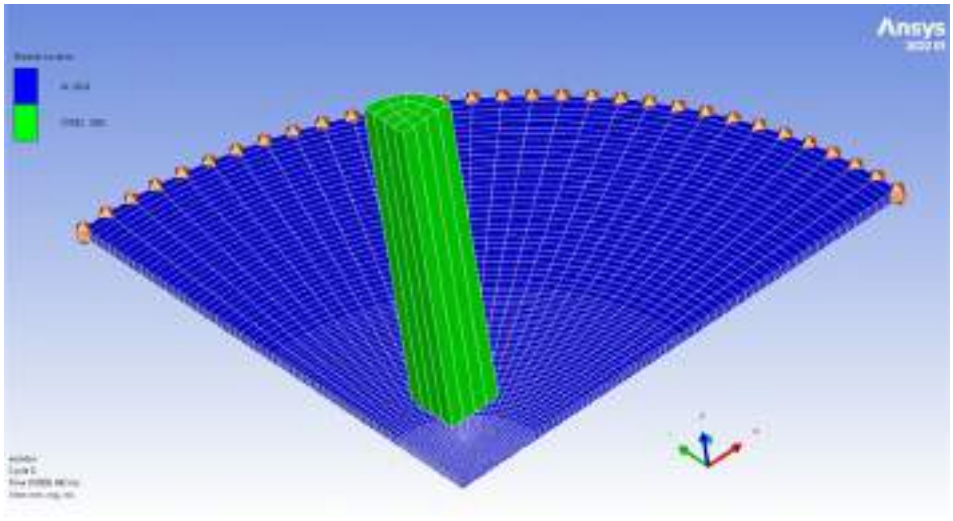

a) Blunt-nosed projectile

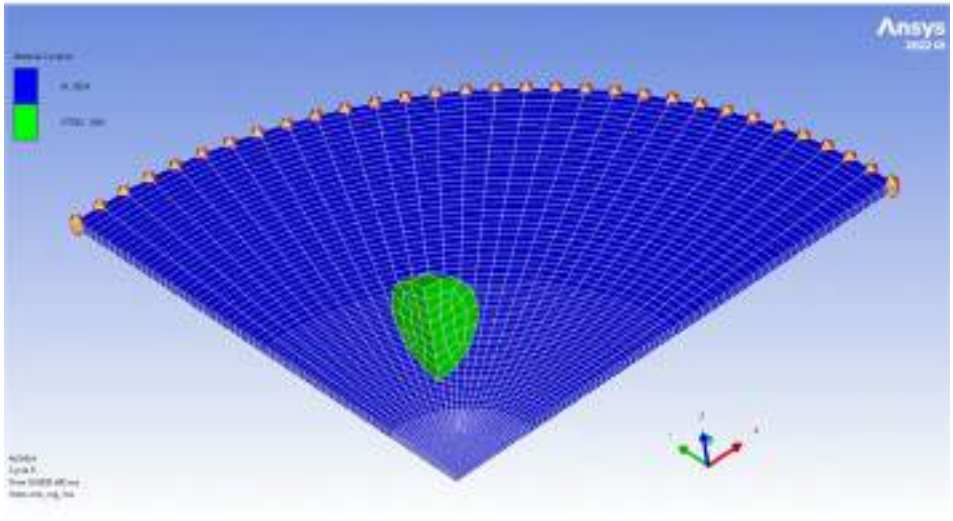

b) Sphere-nosed projectile

Figure 1. Quarter model of the target with a) blunt and b) sphere projectiles with boundary conditions.

the sphere and blunt-nosed projectiles are shown in Figures 6 and 7, respectively. The findings are also given, in more detail, in Tables 1 and 2. The study observed a decline in the ballistic performance of the Al2024 target when subjected to a sphere-nosed projectile as the impact angle of the projectile increased. While the impact angle had minimal effect on the target's ballistic resistance against a blunt-nosed bullet.

3.3. Evaluation of ballistic limit

After conducting a comparative study of the numerical data, a comprehensive evaluation of Al2024's ballistic resistance was undertaken. The ballistic limit was computed numerically using ANSYS Autodyn and theoretically using a model previously proposed by Recht and Ipson [19]. Numerical simulations were performed for the sphere-nosed and blunt projectiles at the predicted impact velocities to estimate the ballistic limit. The residual projectile velocity associated with a certain impact velocity was determined using the Recht-Ipson model presented in the equation below. Tables 1 and 2 provide the impact and residual velocities of both projectiles that were obtained in computational simulations and in the Recht-Ipson model.

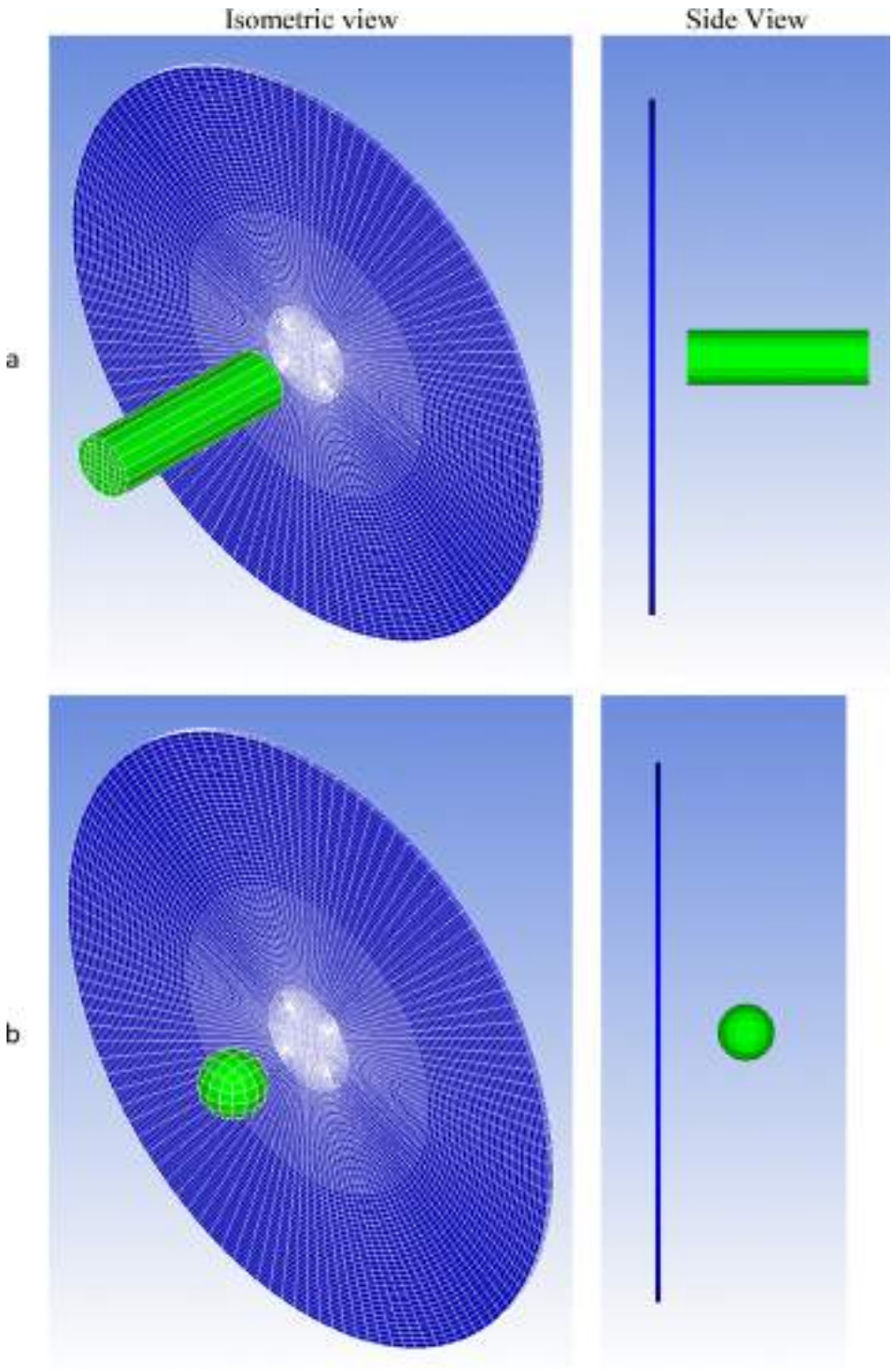

Figure 2. Isometric and side view of the target and projectile a) blunt and b) sphere projectile.

$$V_r = a\left(V_i^p - V_{bl}^p\right)^{\frac{1}{p}}. \quad (1)$$

Where V_r is the residual velocity, a and p are the Recht-Ipson model constants, which are equal to 1 and 2, respectively. V_i and V_{bl} are the initial and ballistic limit velocities, respectively?

The ballistic limit velocity, or V_{50}, may be calculated by taking the average of the greatest projectile velocity that does not cause perforation and the minimum projectile velocity that results in total target perforation. The ballistic limit velocity may increase or decrease depending on the projectile's

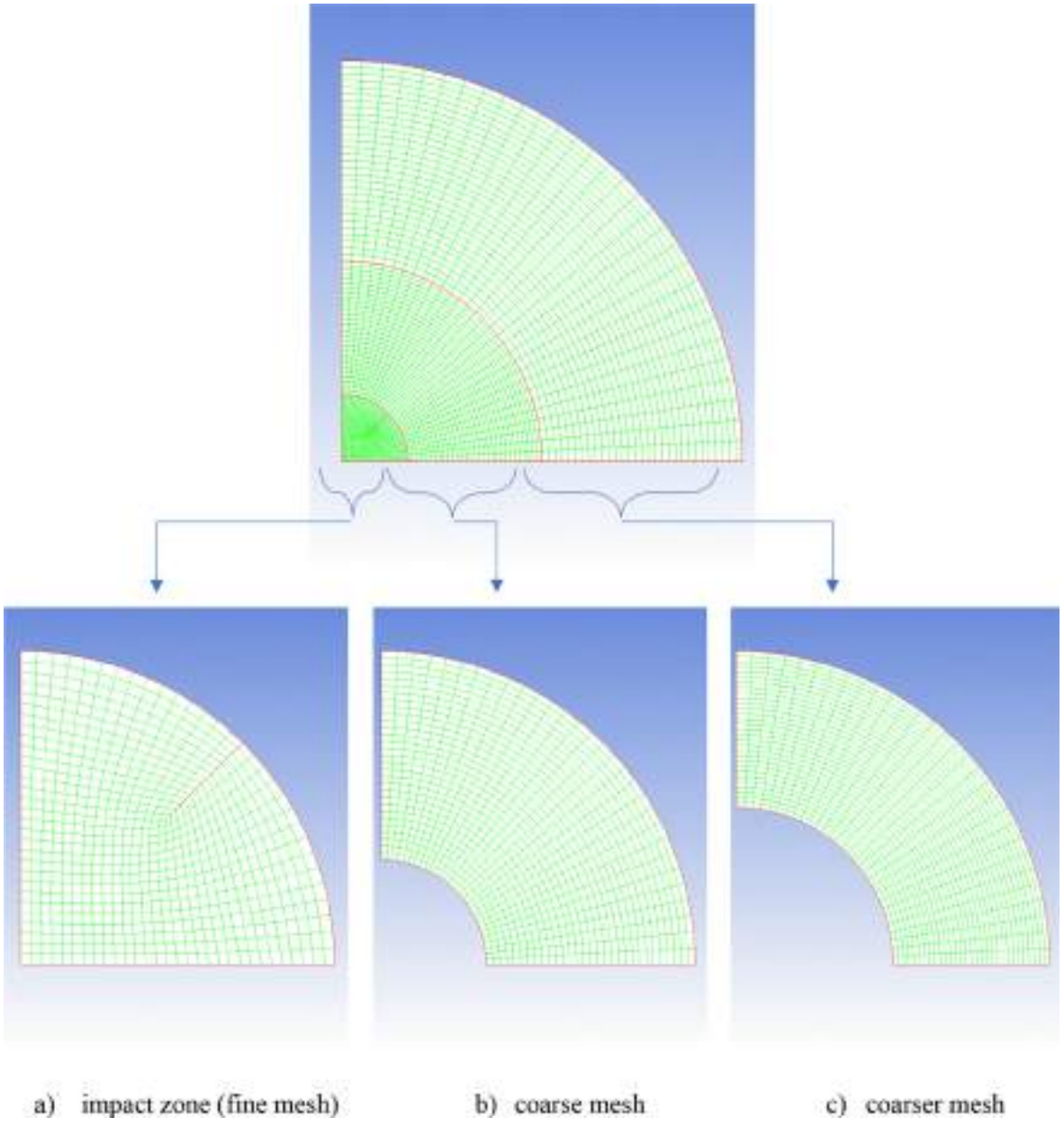

Figure 3. Mesh density zones of the target.

geometrical shape and the value of the impact velocity. For example, the numerical results indicate that the ballistic limit velocity of a sphere is greater in comparison to that of a blunt object. In this investigation, the V_{50} for the 1.27 mm-thickness Al2024 plate target against the normal impact of projectiles with a blunt and spherical-nose was determined to be 33.5 and 128.5 m per second, respectively. Based on the analysis, it can be concluded that the target exhibits the greatest resistance to penetration when subjected to a spherical projectile in comparison to a blunt-nosed projectile.

Table 3 compares the numerical data on the ballistic limit velocity for the blunt and sphere-nosed projectiles. The study determined the ballistic limits against a sphere-nosed projectile for three different obliquity angles: 0°, 15°, and 30°, which were found to be 128.5, 85, and 77.5 m/s, respectively. Hence, it was revealed from Figure 8

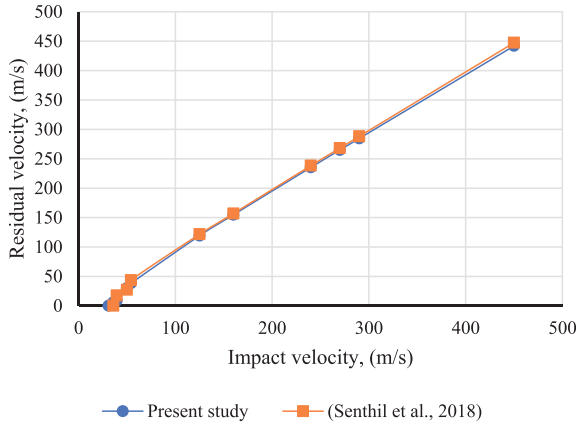

Figure 4. Ballistic limit of Al2024 target against normal impact of blunt nose projectile.

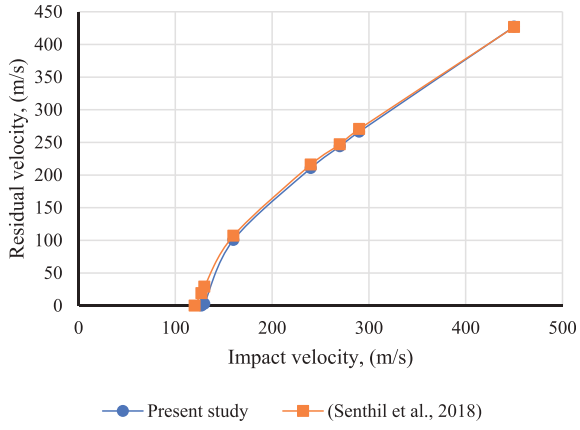

Figure 5. Ballistic limit of Al2024 target against normal impact of sphere nose projectile.

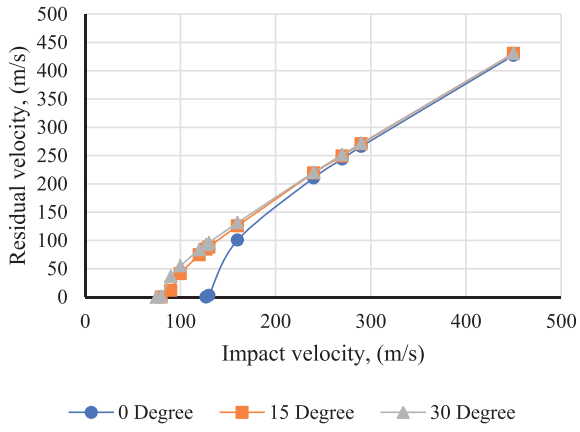

Figure 6. Comparison of ballistic results for the target impacted at various impact angles with a sphere-nosed projectile.

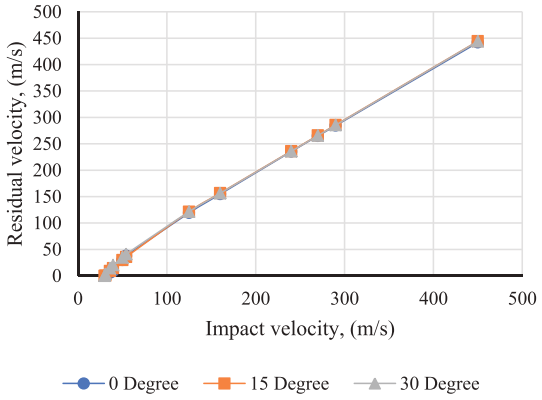

Figure 7. Comparison of ballistic results for the target impacted at various impact angles with a blunt-nosed projectile.

that the ballistic limit exhibited a reduction of 31 % and 38 % at obliquities of 15° and 30°, respectively, compared to the case of normal incidence. It was determined that the ballistic limit velocities of the target when hit by a blunt-nosed projectile at 0°, 15°, and 30° were 33.5, 30.9, and 30.4 m/s, respectively. As shown in Figure 8, the reduction in ballistic performance from the normal angle to 15° and 30° obliquities was negligible, 7.76 % and 9.25 %, respectively.

Figures 9–14 show the computed impact and residual velocity data points and the corresponding Recht-Ipson fit for 1.27 mm thick targets against blunt and sphere nose projectiles at different incident angles.

3.4. Energy absorption analysis

Metals are termed isotropic since their characteristics are the same in all directions. Penetration refers to embedding the projectile into the target, whereas perforation refers to passing the bullet fully through the target. Perforation and penetration models are based on compatibility and conservation laws. The kinetic energy of the bullet is transferred to the plate target when it collides with it. Deforming the target, which consists of stretching, petalling, plugging, and bending, consumes some of the energy [17,20]. Other energies are released as heat and light. The remainder of the energy is transmitted as kinetic energy to the fragments. It is quite difficult to measure or determine each of these energies. In this study, the energy absorption in the projectile was neglected due to insignificant deformations observed during impact. The quantitative evaluation of the energy being absorbed by the Al2024 thin plate target was conducted by numerical simulation in this study.

Table 1. Numerical results of ballistic limit for thin plate target impacted with sphere-nosed projectile.

Obliquity	0°		15°		30°	
Impact velocity (m/s)	Residual velocity (m/s)		Residual velocity (m/s)		Residual velocity (m/s)	
	Numerical results	Recht-Ipson model results	Numerical results	Recht-Ipson model results	Numerical results	Recht-Ipson model results
450	427.15	431.41	430.53	441.31	430.61	443.01
290	266.23	260.22	270.91	276.33	271.83	279.03
270	243.94	237.73	249.15	255.26	251.42	258.18
240	210.59	203.02	219.14	223.28	220.30	226.63
160	100.58	96	125.78	133.63	131.40	139.14
130	2.9	22.72	88.25	95.69	96.17	103.24
127	0	0	84.52	91.57	92.5	99.44
120	–	–	74.62	81.58	83.71	90.33
100	–	–	41.21	47.50	55.06	61.31
90	–	–	11.72	18.87	36.54	43.12
80	–	–	0	0	1	12.61
75	–	–	–	–	0	0

Table 2. Numerical results of ballistic limit for thin plate target impacted with blunt nosed projectile.

Obliquity	0°		15°		30°	
Impact velocity (m/s)	Residual velocity (m/s)		Residual velocity (m/s)		Residual velocity (m/s)	
	Numerical results	Recht-Ipson model results	Numerical results	Recht-Ipson model results	Numerical results	Recht-Ipson model results
450	441.899	448.7513231	444.422	448.9378465	444.108	448.9719813
290	284.512	288.0585878	285.835	288.3490766	285.463	288.4022191
270	264.896	267.9136988	265.976	268.2260055	265.581	268.283134
240	235.367	237.6504786	236.14	238.0025	235.823	238.0668814
160	154.726	156.4536673	156.708	156.9878658	156.37	157.0854545
125	119.171	120.427364	121.45	121.1205598	121.469	121.2470206
54.2	38.2267	42.60739372	35.705	44.52897933	41.0547	44.87181744
50	29.7268	37.11805491	29.875	39.30890484	34.5422	39.69685126
39.5	8.74364	20.92844954	14.3802	24.6056904	20.25	25.22082473
36	5.74235	13.18142633	9.02827	18.47132913	14.3658	19.28315327
31	0	0	0.3	2.487971061	3.40172	6.069596362
30	–	–	0	0	0	0

The classification of elements can be divided into two categories: eroded and uneroded elements. The total energy, denoted as Etotal, is expressed by the following equation [21]:

$$E_{total} = (E_k + E_i)_{eroded} + (E_k + E_i)_{uneroded}. \quad (2)$$

Where E_k is kinetic energy and E_i is internal energy. The kinetic energy that the sphere and blunt bullet lose and the internal rise in the target are shown in Figures 15 and 16, respectively. The results revealed that the increase in internal energy within the target was approximately equivalent to the amount of kinetic energy acquired by the target.

Table 3. Ballistic limit velocities at various obliquities.

Projectile nose shape	Obliquity		
	Ballistic limit, m/s		
	0°	15°	30°
Sphere	128.5	85	77.5
Blunt	33.5	30.9	30.4

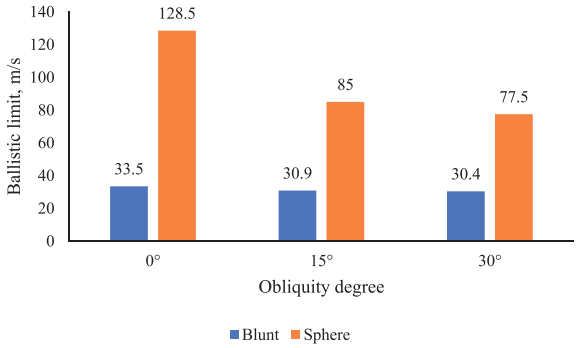

Figure 8. Comparison of ballistic limit velocity obtained from the numerical analysis for blunt and sphere nosed projectile.

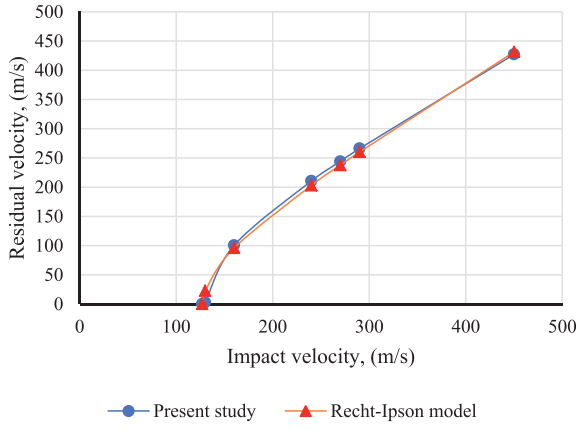

Figure 9. Ballistic limit for the target impacted at normal obliquity with sphere-nosed projectile.

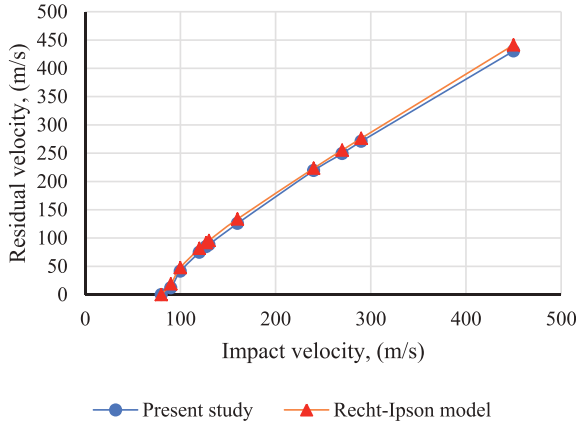

Figure 10. Ballistic limit for the target impacted at 15° obliquity with sphere-nosed projectile.

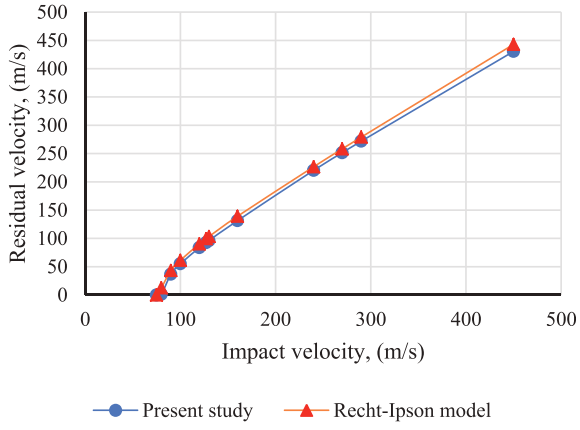

Figure 11. Ballistic limit for the target impacted at 30° obliquity with sphere-nosed projectile.

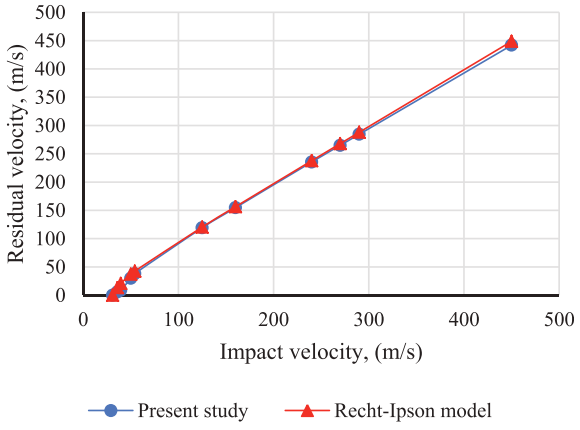

Figure 12. Ballistic limit for the target impacted at normal obliquity with blunt-nosed projectile.

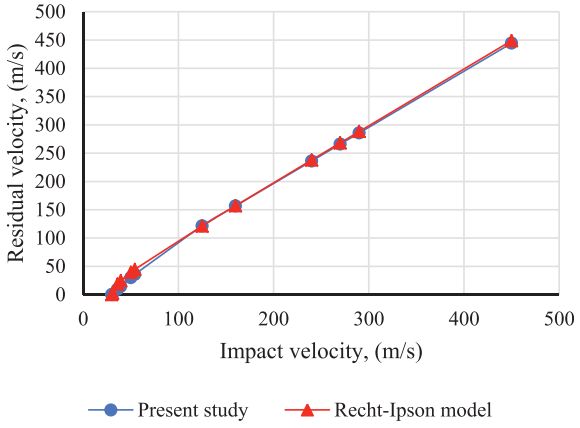

Figure 13. Ballistic limit for the target impacted at 15° obliquity with blunt-nosed projectile.

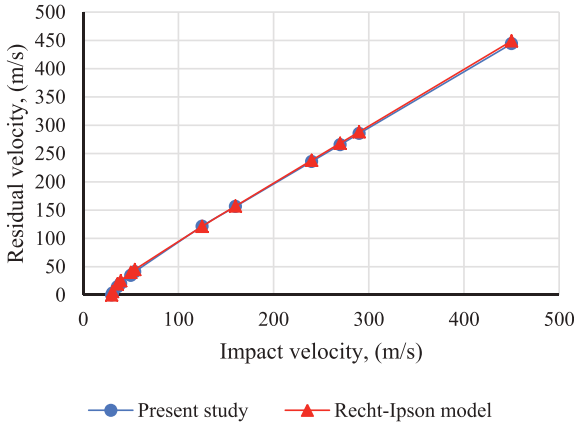

Figure 14. Ballistic limit for the target impacted at 30° obliquity with blunt-nosed projectile.

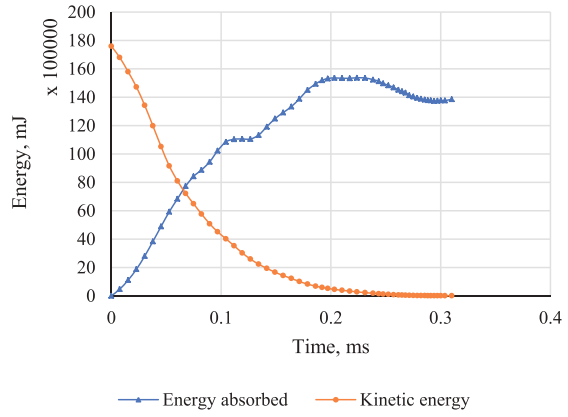

a) 0°

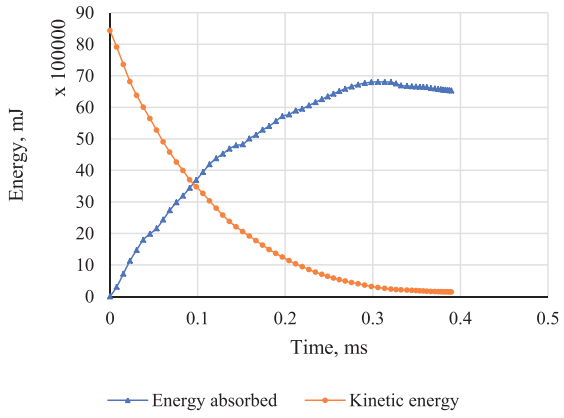

b) 15°

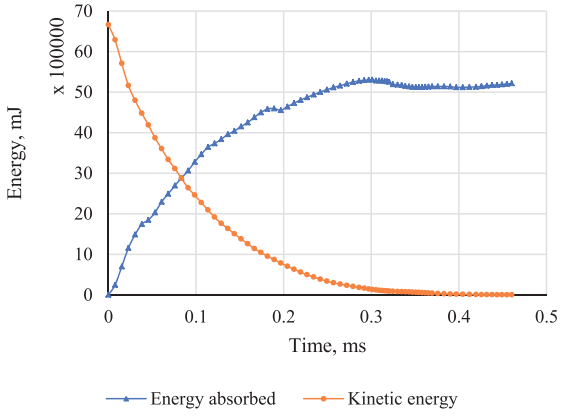

c) 30°

Figure 15. Energies versus time for target impacted with sphere-nosed projectile at a) 0°, b) 15° and c) 30° obliquities.

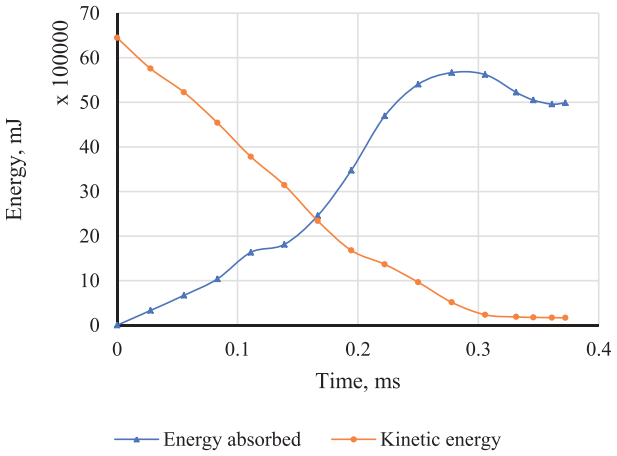

a) 0°

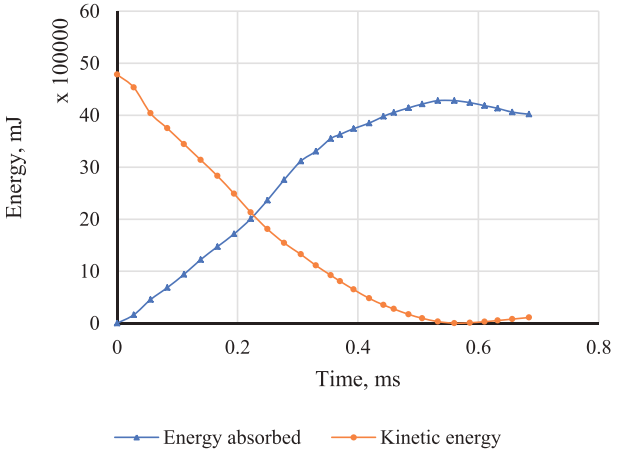

b) 15°

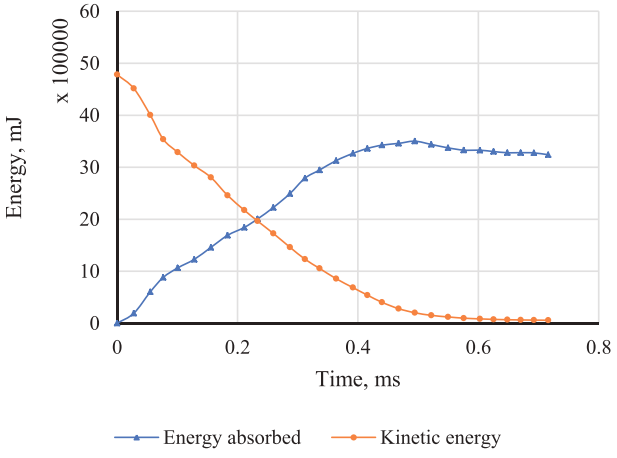

a) 30°

Figure 16. Energies versus time for target impacted with blunt-nosed projectile at a) 0°, b) 15° and c) 30° obliquities.

4. Conclusions

The main goal of the current study was to evaluate the impact performance of the Al2024 target against blunt and sphere-nosed projectiles at varying impact angles of 0°, 15°, and 30°. The evaluation was conducted through a numerical study using ANSYS Autodyn, and the results were compared with previous experimental and numerical studies. The most obvious finding to emerge from this study is that the target has the greatest ballistic limit against sphere projectiles, followed by projectiles with blunt projectiles. At normal incident impact, the ballistic limit of a sphere projectile was approximately 117 % greater than that of a blunt projectile. However, this difference decreased with increasing incident angle, where the value decreased to 93 % and 87 % at 15° and 30° impact angles, respectively. The results indicated that the increase in internal energy within the target was roughly equivalent to its kinetic energy.

Conflicts of interest

The author has no conflicts of interest to declare.

Acknowledgments

The author would like to thank Erbil Polytechnic University in Erbil, Iraq, for its support.

References

[1] Starke EA, Staley JT. Application of modern aluminium alloys to aircraft. In: Fundamentals of Aluminium Metallurgy: Production, Processing and Applications [Internet]. Woodhead Publishing Limited; 2010. p. 747–83. Available from: https://doi.org/10.1533/9780857090256.3.747.

[2] Johnson GR, Cook WH. Fracture characteristics of three metals subjected to various strains, strain rates, temperatures and pressures. Eng Fract Mech 1985;21(1):31–48. Available at: https://doi.org/10.1016/0013-7944(85)90052-9.

[3] Iqbal MA, Senthil K, Bhargava P, Gupta NK. The characterization and ballistic evaluation of mild steel. Int J Impact Eng [Internet] 2015;78:98–113. Available from: https://doi.org/10.1016/j.ijimpeng.2014.12.006.

[4] Alfaro-Bou E, Thomson RG. Ballistic Limit of Aluminum Plates Determined by an Exploding Foil Gun Technique. WASHINGTON. 1967.

[5] Goldsmith W, Finnegan SA. Normal and oblique impact of cylindro-conical and cylindrical projectiles on metallic plates. Int J Impact Eng 1986;4(2):83–105. Available at: https://doi.org/10.1016/0734-743X(86)90010-2.

[6] Gogolowski RP, Morgan BR. Ballistic experiments with titanium and aluminum targets. In: FAA Rep. No. DOT/FAA/AR-01/21, U.S. Department of Transportation, Federal Aviation Administration, Washington, D.C. 20591; 2001.

[7] Levy N, Goldsmith W. Normal impact and perforation of thin plates by hemispherically tipped projectiles — II. Experimental results. Int J Impact Eng 1984;2(4):299–324. Available at: https://doi.org/10.1016/0734-743X(84)90020-4.

[8] Kelley S, Johnson G. Statistical testing of aircraft materials for transport airplane rotor burst fragment shielding. In: FAA Rep. No. DOT/FAA/AR-06/9, U.S. Department of Transportation, Federal Aviation Administration, Washington, D.C. 20591; 2006.

[9] Gupta NK, Iqbal MA, Sekhon GS. Effect of projectile nose shape, impact velocity and target thickness on deformation behavior of aluminum plates. Int J Solids Struct 2007;44(10):3411–39. Available at: https://doi.org/10.1016/j.ijsolstr.2006.09.034.

[10] Buyuk M, Kan S. Explicit finite element analysis of 2024-T3/T351 aluminum material under impact loading for airplane engine containment and fragment shielding. Earth Sp Conf 2008 Proc 11th Aerosp Div Int Conf Eng Sci Constr Oper Challenging Environ 2008;323. Available at: https://doi.org/10.1061/(asce)0893-1321(2009)22:3(287).

[11] Hub J, Komenda J, Novák M. Ballistic limit evaluation for impact of pistol projectile 9 mm luger on aircraft skin metal plate. Adv Mil Technol 2012;7(1):21–9.

[12] Jones N, Paik JK. Impact perforation of steel plates. Ships Offshore Struct 2013;8(5):579–96. Available at: https://doi.org/10.1080/17445302.2012.704163.

[13] Jones N, Paik JK. Impact perforation of aluminium alloy plates. Int J Impact Eng [Internet] 2012;48:46–53. Available from: https://doi.org/10.1016/j.ijimpeng.2011.05.007.

[14] Zhan T, Li J, Lv S, Chen Z. Residual velocity for the truncated ogival-nose projectile into stiffened plates. Ships Offshore Struct 2015;11(6):636–44. Available from: https://doi.org/10.1080/17445302.2015.1041441.

[15] Senthil K, Arindam B, Mittal R, Iqbal MA. Numerical investigations on impact of ogive nosed projectiles on thin plates. Indian J Sci Technol 2016;9(S1):1–6. Available at: https://doi.org/10.17485/ijst/2016/v9is1/99243.

[16] Gara N, Ramachandran V, Rengaswamy J. Analytical and FEM analyses of high-speed impact behaviour of Al 2024 alloy. Aerospace 2021;8(10):0–21. Available at: https://doi.org/10.3390/aerospace8100281.

[17] Mohotti D, Ngo T, Raman SN, Ali M, Mendis P. Plastic deformation of polyurea coated composite aluminium plates subjected to low velocity impact. Mater Des [Internet] 2014;56:696–713. Available from: https://doi.org/10.1016/j.matdes.2013.11.063.

[18] Senthil K, Iqbal MA, Arindam B, Mittal R, Gupta NK. Ballistic resistance of 2024 aluminium plates against hemispherical, sphere and blunt nose projectiles. Thin-Walled Struct 2018;126(February 2017):94–105. Available at: https://doi.org/10.1016/j.tws.2017.02.028.

[19] Recht RF, Ipson TW. Ballistic perforation dynamics. J Appl Mech Trans ASME 1963;30(3):384–90. Available at: https://doi.org/10.1115/1.3636566.

[20] Barrett S. Ballistic Properties of Projectile Material. 2016.

[21] Yu H, Fan Q, Zhu X. Effect of the layer sequence on the ballistic performance and failure mechanism of Ti6Al4V/CP-Ti laminated composite armor. Materials (Basel) 2020;13(17):1–14. Available at: https://doi.org/10.3390/ma13173886.